Journal of
Nanomedicine & Nanotechnology

Desai et al., J Nanomed Nanotechnol 2015, 6:6
DOI: 10.4172/2157-7439.1000338

Research Article Open Access

Chemically Grown MoO_3 Nanorods for Antibacterial Activity Study

Neha Desai[1], Sawanta Mali[2], Vijay Kondalkar[1], Rahul Mane[1], Chang Hong[2] and Popatrao Bhosale[1]*

[1]*Materials Research Laboratory, Department of Chemistry, Shivaji University, Kolhapur, India*
[2]*School of Applied Chemical Engineering, Chonnam National University, Gwangju, South Korea*

Abstract

In the present investigation, sea urchin like morphology of h-MoO_3 nanorods are successfully synthesized by chemical bath deposition (CBD) technique. The thermal stability, structural details, morphology and compositional analysis of MoO_3 was done using thermogravimetry (TGA), X-ray diffraction (XRD), scanning electron microscopy (SEM), high resolution transmission electron microscopy (HR-TEM), selected area electron diffraction (SAED) and X-ray photoelectron spectroscopy (XPS) techniques respectively. The thermal analysis reveals presence of sharp exothermic peak at 409ºC indicating irreversible phase transition. X-ray diffraction pattern showed hexagonal to orthorhombic phase transition after annealing at 450ºC. As synthesized h-MoO_3 shows well oriented hexagonal rods with sea urchin like architecture while that of annealed MoO_3 sample revealed 2D layer by layer growth. The SAED pattern confirms single crystalline nature of as synthesized h-MoO_3 and polycrystalline nature of annealed α-MoO_3. While XPS study of both confirms Mo^{+6} and O^{2-} oxidation states of elements. Furthermore, characteristic antibacterial properties of h-MoO_3 and α- MoO_3 against gram positive *Bacillus megaterium*, *Streptococcus aureus* and gram negative *Escherichia coli* is noted.

Keywords: MoO_3; CBD; Hexagonal rods; XPS; HR-TEM

Introduction

The transition metal oxides (TMOs) are attracting a great deal of attention in the field of material science due to its variety of crystal phases and properties. The nano crystalline TMOs such as TiO_2, WO_3, MoO_3 and ZnO are the most widely studied by various researchers all over the world [1-8]. Among the TMOs, molybdenum trioxide (MoO_3) exhibits better intercalation chemistry with unique chemical, electrochemical, electronic and catalytic properties. The MoO_3 exhibits variety of crystal phases such as orthorhombic (α-MoO_3), monoclinic (β-MoO_3) and hexagonal (h-MoO_3) [9,10], out of these orthorhombic is thermodynamically more stable while monoclinic and hexagonal forms are metastable in nature. The orthorhombic MoO_3 phase possess a unique 2 dimensional (2D) layered structure in which each layer is consists of two sub layers stacked along (010) direction [11]. The h-MoO_3 is constructed by the zig-zag chains of [MoO_6] octahedral which are interlinked together through cis position giving a one dimensional tunnel structure [12]. The tunnel structure facilitates electron-hole pair separation under irradiation and enhances the photochromic performance. As a result of this, MoO_3 have potential applications in the field of photocatalysis [13], electrochromism [14,15], lithium ion batteries [16,17], light emitting diodes etc. [18]. Besides MoO_3 show polymorphism, therefore can be synthesized in different morphologies such as nanofibers [19], nanorods [20], nanobelts [21], nanowires [22] for various applications.

Recently, in addition to photo electrochemical properties, TMOs nanoparticles have been investigated for their antimicrobial activity due to their extra stability and non toxic nature. Antibacterial agents are very important in the textile industries, water disinfection, medicine and food packing. Number of organic substances shows the antibacterial activity but most of them are toxic in nature. Hence in the recent years there is growing demand for metal oxide nanoparticles as antibacterial agent due to their high stability and non toxic nature [23-25]. Recently Zollfrank et al. reported that antimicrobial activity of transition metal acid MoO_3 is related to their surface acidity involving the intermediate formation of molybdic acid [26]. The toxicity of MoO_3 towards pathogenic bacteria has been studied by K. Krishnamoorthy et al. [27]. As per this report prepared MoO_3 nanoplates exhibit good antibacterial activity against 4 tested bacterial species *E. coli, S. Typhimurium, B. Subtilis, E. Faecalis* .

In this view we are reporting synthesis of nanocrystalline h- MoO_3 using a simple and low cost chemical bath deposition technique studies on its phase transition and characteristic antibacterial properties exhibited towards gram positive and gram negative bacteria.

Experimental

Materials

All the precursor chemicals used for the synthesis were of AR (Analytical reagent) grade and directly purchased. The ammonium heptamolybdate tetrahydrate (AHM) $(NH_4)_6Mo_7O_{24}.4H_2O$ (Merck, 99%) and concentrated nitric acid HNO_3 (Merck) were used for the synthesis of MoO_3.

Method

The nanocrystalline MoO_3 was synthesized by chemical bath deposition technique. Various experimental runs were carried out for concentrations such as 0.025 M, 0.05 M and 0.075 M solutions of AHM in order to optimize the preparative parameter. For 0.025 M and 0.075 M AHM concentration, a sluggish and bulky precipitate was obtained. While for 0.05M, white coloured crystalline precipitate was obtained. In a typical synthesis, 15 mL of 0.05 M AHM solution was taken in a reaction bath. The temperature of reaction bath was increased slowly up to 50°C. To this 5 mL of conc. HNO_3 was added drop wise with

***Corresponding author:** Popatrao Bhosale, Materials Research Laboratory, Department of Chemistry, Shivaji University, Kolhapur-416004, India, Tel: 91-231-2609338; E-mail: p_n_bhosale@rediffmail.com

Received October 13, 2015; **Accepted** November 10, 2015; **Published** November 20, 2015

Citation: Desai N, Mali S, Kondalkar V, Mane R, Hong C, et al. (2015) Chemically Grown MoO_3 Nanorods for Antibacterial Activity Study. J Nanomed Nanotechnol 6: 338. doi:10.4172/2157-7439.1000338

constant stirring to obtain a clear solution. This clear solution was then stirred for 15 min thereafter the temperature of reaction bath was maintained to 70°C, at this temperature formation of initial seed nuclei can be observed by naked eye. The reaction bath was maintained at 70°C for 30 minutes to obtain the white coloured precipitate of h-MoO_3. Finally, the precipitate of h-MoO_3 was filtered off with deionized water and then dried in constant temperature oven at 110°C for an hour.

Characterization of h-MoO_3

The thermal analysis was carried out upto 1000°C in nitrogen atmosphere using TGA-DSC model (SDT Q600 V20.9 Build 20) at a scanning rate of 10°C/min. The phase identification of synthesized sample was performed by X- ray diffractometer (Brucker AXS, D_8 model) at a scanning rate of 0.2° per min in the range of 20° to 80° with Cu ($K_{\alpha 1}$ target at 1.54 Å). The surface morphology was examined by field emission scanning electron microscopy (FE-SEM) (Hitachi S 4700) and scanning electron microscopy (SEM) (JEOL-JSM-6360A) equipped with energy dispersive X-ray analyser (EDS). Transmission electron microscopy (TEM), high resolution transmission electron microscopy (HRTEM) and selected area electron diffraction (SAED) were performed with a transmission electron microscope (TECNAI F20 Philips). The surface area analysis was carried out in nitrogen atmosphere. An X-ray photoelectron study to confirm oxidation state of molybdenum and oxygen in both the phases of MoO_3 was carried out using XPS (VG multilab 2000- Thermoscientific, USA, k-alpha) with a multi channel detector. For the SEM analysis of *S. Aureus*, aliquots of 1mL of controls and cells exposed to α-MoO_3. After drying the samples overnight at room temperature specimens were further sputter coated with gold. SEM images were then acquired by Field emission scanning electron microscope.

Antibacterial activity

The antibacterial activity of MoO_3 was evaluated against gram positive bacteria like *Bacillus megaterium, Streptococcus aureus* and gram negative bacteria *Escherchia coli* by using cup plate method [28]. The cups were prepared in the nutrient agar medium with the help of sterilized cork borer and it was seeded with the 18 h old broth culture of each organism. The solution of each test compound was made in hot distilled water at different concentration such as 10^{-1}, 10^{-2} and 10^{-3} mg/ml and added to the cups. After inoculation of test samples of MoO_3, the Petri plates were incubated at 37°C for 48 h. The zone of inhibition was recorded in mm after 48 h. Ciprofloxacin was used as a standard control to represent zone of inhibition.

Results and Discussions

Growth and reaction mechanism

The properties of the nanomaterial are largely dependent on their growth mechanism. For the synthesis of h-MoO_3 all the preparative parameters such as concentration of precursors, temperature, time, choice of precursors were optimized at initial stages to get desired morphology. The $(NH_4)_6Mo_7O_{24}.4H_2O$ (AHM) and conc. HNO_3 acts as reaction partner for the formation of MoO_3. The formation of MoO_3 can be understand as per the following reaction mechanism [29].

$$(NH_4)_6Mo_7O_{24}.4H_2O \longrightarrow 6\,NH_4^+ + Mo_7O_{24} + 4H_2O$$

$$6HNO_3 \longrightarrow 6H^+ + 6NO_3^-$$

$$6\,NH_4^+ + 6NO_3^- \longrightarrow 6\,NH_4NO_3$$

$$Mo_7O_{24}^{-6} + 6H^+ \longrightarrow 7MoO_3 + 3\,H_2O$$

$$(NH_4)_6Mo_7O_{24}.4H_2O\,(aq.) + 6HNO_3 \longrightarrow 7MoO_3 + 6\,NH_4NO_3\,(aq.) + 7\,H_2O$$

As per the above reaction mechanism, dissociation of AHM takes place to produce $6NH_4^+$ and $Mo_7O_{24}^{-6}$ ion. In the next step concentrated nitric acid ionizes to H^+ and NO_3^- ions. The ionisation of AHM released NH_4^+ and NO_3^- ions combine together to form NH_4NO_3. Finally solid MoO_3 get separated as microcrystallites in acidic medium.

As the formation of MoO_3 follows the principle of Ostwald ripening law [30]. The growth mechanism for the formation of MoO_3 is graphically represented in the Figure 1.

According to the Ostwald ripening phenomena initially there is formation of seed nucleus. Once these seed nucleus attain critical size they act as nucleation centres and favours growth of hexagonal rods. The smaller crystallites are kinetically stable while the larger crystallites are thermodynamically stable. The kinetically stable smaller crystallite sacrifices themselves to form thermodynamically stable larger crystallites in accordance with Ostwald ripening phenomenon. Hence at 70°C when the growth of multinucleation centre was completed resulting in the formation of larger crystallites. Further these larger crystallites attain directional growth to form 1D hexagonal rod. So in the present investigation, hexagonal rods assembled themselves to form sea urchin like architecture.

Thermal analysis

TGA-DSC analysis was performed in order to understand the thermal behaviour of MoO_3. Figure 2 shows TGA curve in the temperature range of 25°C to 1000°C for h-MoO_3.

Below 500°C, three weight losses were observed. The first weight loss equivalent to 5.375% in temperature range of 50°C -150°C was due to the desorption of physically adsorbed water molecules at the surface of h-MoO_3 sample. The next weight loss observed at 350°C

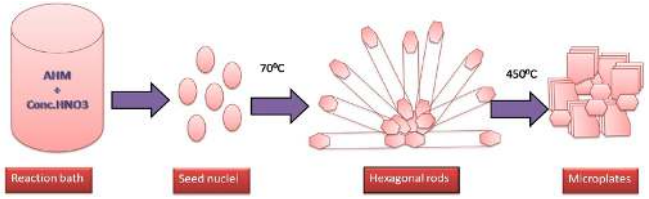

Figure 1: Graphical Representation of Growth Mechanism.

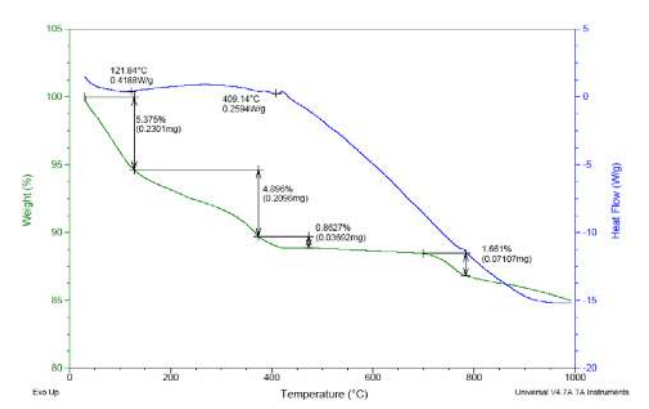

Figure 2: Thermal analysis of as synthesized MoO_3.

corresponds to the loss of ammonia and other nitrates. The sharp exothermic peak at 409°C indicates the irreversible phase transition from hexagonal to orthorhombic MoO_3. We observe no weight loss in 450-700°C temperature range. It indicates the formation of thermodynamically stable α-MoO_3. Therefore according to the TGA-DSC analysis it is clear that the h-MoO_3 is a metastable phase while α-MoO_3 is a thermodynamically stable phase [31].

Structural analysis

The phase identification of MoO_3 sample was carried out by using XRD. Figure 3a shows diffraction pattern of as synthesized MoO_3 sample.

The XRD pattern of as synthesized MoO_3 was well indexed with JCPDS Card No.21-0569 [32]. We observe no secondary diffraction peaks due to impurities or other phases indicating presence of single, hexagonal phase of MoO_3. The lattice parameters 'a' and 'c' of as synthesized h-MoO_3 were determined from the standard equation no.1.

$$\frac{1}{d^2}=\frac{4}{3}\left[\frac{h^2+hk+k^2}{a^2}\right]+\frac{1^2}{c^2} \quad (1)$$

The calculated values of lattice parameters were a = 10.48 Å and c = 14.91 Å which are in good agreement with standard values. The crystallite size was calculated by using the Debye-Scherrer equation,

$$D=\frac{0.9\lambda}{\beta\cos\theta} \quad (2)$$

The crystallite size calculated from the most intense (210) peak at 2θ = 25.88 was 36.63 nm. The 'as synthesized' h-MoO_3 was annealed at 450°C for 4 hours. The annealing changes colour of the sample from whitish to grey. Figure 3b shows diffraction pattern obtained for annealed MoO_3 sample. The sharp intense diffraction peaks in the XRD pattern of the annealed MoO_3 sample were well matched with JCPDS Card No.05-0508 [33]. Furthermore, due to absence of impurities no secondary diffraction peaks were observed. This confirmed the formation of single phase and crystalline orthorhombic molybdenum trioxide. The calculated values of lattice parameters were a = 3.961, b = 13.87 Å and c = 3.69 Å using Equation no.3,

$$\frac{1}{d^2}=\frac{h^2}{a^2}+\frac{k^2}{b^2}+\frac{1^2}{c^2} \quad (3)$$

The crystallite size calculated from the (021) planes (2θ = 25.79) using Debye-Scherrer equation is found to be 66. An increase in the crystallite size was observed from XRD pattern as a result of annealing.

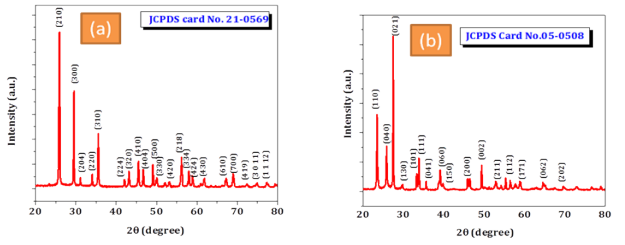

Figure 3: (a) XRD pattern of as synthesized sample.(b)XRD pattern of annealed sample.

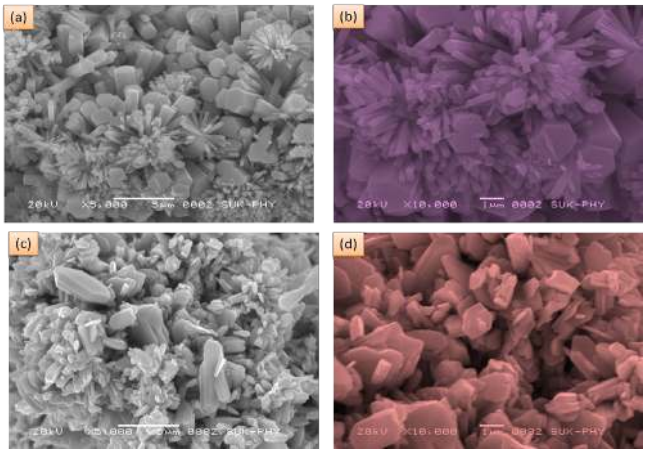

Figure 4: SEM of h-MoO_3(a and b), SEM of α-MoO_3(c and d).

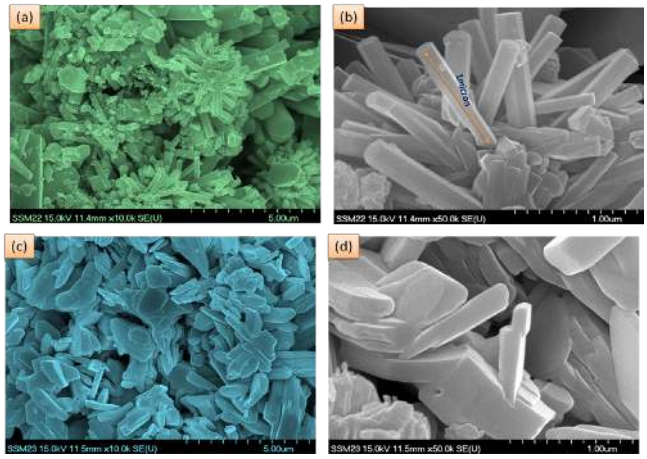

Figure 5: FE-SEM of h-MoO_3 (a and b), FE-SEM of α-MoO_3 (c and d).

Morphological analysis

The surface morphology of both h-MoO_3 and α-MoO_3 was characterized by SEM and FESEM analysis. Figure 4a and 4b clearly indicates presence of 1D hexagonal rods. These rods are well oriented and assembled to form a 'sea urchin' like architecture. The sea urchin like structure has average diameter of about 3 micron. The sea urchin like structure is believed to be due to nucleation, growth and attachment mode. The MoO_3 exhibits 3 polymorphic forms α-MoO_3, β-MoO_3 and h-MoO_3. Among all these polymorphic forms h-MoO_3 exhibits superior physical and chemical properties over the other. Further growth of well oriented hexagonal rods can occur to give 2D structure. After annealing at 450°C 1D hexagonal nanorods gets converted into 2D plate like structure for α - MoO_3 as observed from Figure 4c and 4d.

To give more emphasis on morphological features of MoO_3, FESEM images are shown in Figure 5. From Figure 5a and 5b of h-MoO_3 it is observed that 1D rods are monodispersed having average length of about 1 micron. The individual rods are polygon crystals with hexagonal cross section and well developed facets without any impurity [34]. Figure 5c and 5d indicates 2D plate like structure of α-MoO_3. The α-MoO_3 has tendency to undergo layer by layer deposition [35]. The plate like structure shows presence of thinner sub plates intercalated

within it. Thus MoO_3 exhibits good intercalation chemistry and form a basis for good morphology.

In order to determine detail crystal structure and to gain more insight into the morphological aspects of as synthesized h-MoO_3 and annealed α-MoO_3 HRTEM analysis was carried as shown in Figure 6, Figure 6a displays TEM image of h-MoO_3. It clearly indicates presence of single nanorod having a length of about 1 micrometer. This image is well consistent with FESEM results. The Figure 6b shows selected area electron diffraction (SAED) pattern of h-MoO_3. The bright dotted SAED pattern confirms single crystalline nature of h-MoO_3 [36].

Furthermore Figure 6c shows TEM image for α-MoO_3. It reveals presence of nanoplate like structure having number of sub plates intercalated within it. This plate like structure has a average diameter of about 100 nm. This result well matches with morphological study. Figure 6d shows SAED pattern of α-MoO_3. The distinct bright rings pattern indicates polycrystalline nature of α-MoO_3 [37].

Surface area analysis

The BET surface area and pore volume were evaluated by using nitrogen adsorption and desorption isotherm. The BET data of both as synthesized h-MoO_3 and annealed α-MoO_3 is presented in the table. From BET analysis, it can be observed that both surface area and pore volume was decreased after annealing. As a result of annealing smaller crystallites assembled to form larger crystallites [38,39]. Moreover XRD study reveals that crystallite size also increases from 36 to 63 nm after annealing. Therefore increase in the crystallite size results in decrease in surface area (Table 1).

Compositional analysis

The quantitative analysis of both as synthesized and annealed MoO_3 was carried out by using EDS technique. Figure 7 shows a typical EDS spectrum of h-MoO_3 and α-MoO_3. The prominent peaks observed at 2.4 keV and 0.52 keV confirming the presence of Mo^{3+} and O^{2-} elements respectively. The inset table shows expected and observed atomic percentage of molybdenum and oxygen. The observed atomic percentage of Mo^{3+} and O^{2-} are in good agreement with theoretical atomic percentage of respective elements.

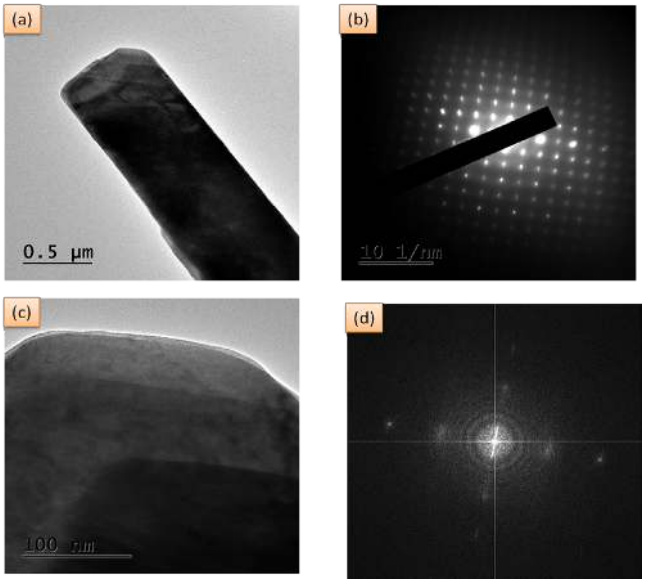

Figure 6: TEM image of h-MoO_3 (a), SAED pattern of h-MoO_3 (b), TEM image of α-MoO_3 (c) and SAED pattern of α-MoO_3 (d)

Sample	SBET(m^2/g)	VTotal (mL/g)
h-MoO_3	3.58	0.0063
α -MoO_3	6.16	0.0095

Table 1: Surface area and pore volume of h-MoO_3 and α-MoO_3.

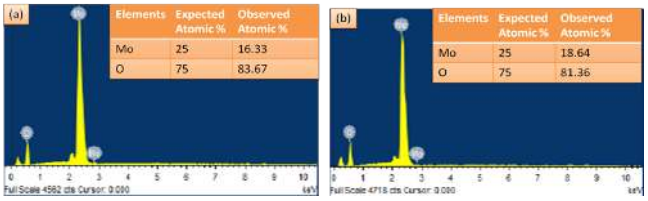

Figure 7: EDS spectrum of h-MoO_3 (a) and EDS spectrum of α-MoO_3(b)

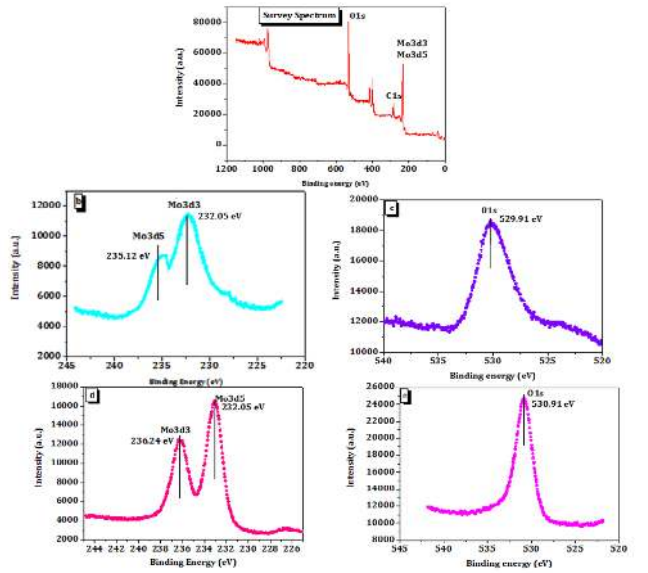

Figure 8:- XPS Survey spectrum (a), 3d core level spectrum of h-MoO_3 (b) O1S core level spectrum of h-MoO_3(c), 3d core level spectrum of α-MoO_3 (d), O1S core level spectrum of α-MoO_3 (e).

The X-ray photoelectron spectroscopy was used to determine the chemical bonding and surface composition of h-MoO_3 and α-MoO_3 the samples. The XPS survey spectrum of MoO_3 was shown in the Figure 8a. The survey spectrum shows peaks for Mo, O and C. The C 1S peak at 284.6 eV is used as reference. The binding energies of all other elements were calibrated using C 1S peak. The Mo 3d core level spectrum of as synthesized h-MoO_3 shows doublets at 235.12eV and 232.05 eV from Figure 8b [40] which is attributed to B.E. of the $3d^3$ and $3d^5$ orbital electrons of Mo^{6+}. The energy difference between them is 3.07 eV which is for h- MoO_3. The O1S core level spectrum of h-MoO_3 exhibit binding energy at 529.91 eV which is due to presence of lattice oxygen in MoO_3 as shown in Figure 8c. The Mo3d core level spectrum of annealed α-MoO_3 shows spin orbit doublet at 236.24 eV and 233.07 eV for $Mo3d_{3/2}$ and $Mo3d_{5/2}$ respectively confirming +6 oxidation state of molybdenum as shown in Figure 8d [41,42]. The energy difference

between the doublets is 3.17eV for α-MoO_3. The O1S core level spectra of α-MoO_3 shows peak at 530.91 eV which is attributed to the presence of oxygen in Mo-O-Mo bonding as shown in Figure 8e. This confirms -2 oxidation state for oxygen. As compared to the h-MoO_3, increase in the binding energy was observed for $3d^3$ and $3d^5$ orbital electrons of Mo^{+6}. in α-MoO_3 Similarly, increase is also observed for the B.E. value of O1S spectra of α-MoO_3.

Antibacterial activity study

Cup plate method [28] was used to conduct antibacterial activity against gram positive bacteria like *Bacillus megaterium*, *Streptococcus aureus* and gram negative bacteria *Escherchia coli* respectively. The standard drug used for reference was ciprofloxacin. The zone of inhibition in mm observed for various bacterial strains are shown in Table 2.

The presence of inhibition zone revealed the biocidal activity of MoO_3 nanoparticles. From this result, we conclude that both the phases of MoO_3 are reactive against gram positive *Bacillus megaterium*, *Streptococcus aureus*. However α-MoO_3 only shows antibacterial activity against *E. coli* bacteria. In order to explain detail mechanism of antibacterial activity it is necessary to understand the interaction between nanomaterial and bacterial cell wall. The cell wall of gram negative *E.coli* is complicated one due to the presence of outer lipopolysaccharide and inner peptidoglycin layer [43]. On the contrary, the cell wall of gram positive *Bacillus megaterium* is simple one with a thick layer of peptidioglycan. This layer contains chains of amino acids and carbohydrates of repeated units. Nanoparticles react with the amide, phosphate and carboxyl groups thereby disrupting the cell processes. All these surface interactions between the cell wall and nanoparticales lead to the destruction of the cell wall [44]. So the antibacterial activity against gram positive bacteria was shown by both the phases of MoO_3. Along with this the size, shape, structure and composition of nanomaterials also plays a crucial role in the antibacterial activity [45]. The nano-biointerface is an important phenomenon for the understanding of antibacterial activity [23-26]. The interface between a nanoparticle and any living moiety or biomaterial is termed as nanobiointerface. This phenomenon is explained graphically in Figure 9.

In our case there is a interaction between MoO_3 nanoparticles and bacterial strains. The bactericidal effect of the metal nanoparticle has been attributed to their small size and high surface to volume ratio. As per the literature survey the antibacterial activity of metal oxide nanoparticles is due to membrane or oxidative stress mechanism. If there is a direct interaction between the nanomaterials and bacterial species then membrane stress mechanism occurs. The cell death may occur due to excess level of oxygen species after exposure to nanomaterials following the oxidative stress mechanism. However, the

Zone of Inhibition (mm)			
Samples	**Gram positive**	**Gram negative**	
h-MoO_3	Streptococcus aureus	Bacillus megaterium	Escherchia coli
1-Oct	2	4	-
2-Oct	-	7	-
3-Oct	3	13	-
α-MoO_3			
1-Oct	3	6	15
2-Oct	2	8	18
3-Oct	-	10	9

Table 2: Antibacterial activity of h-MoO_3 and α-MoO_3.

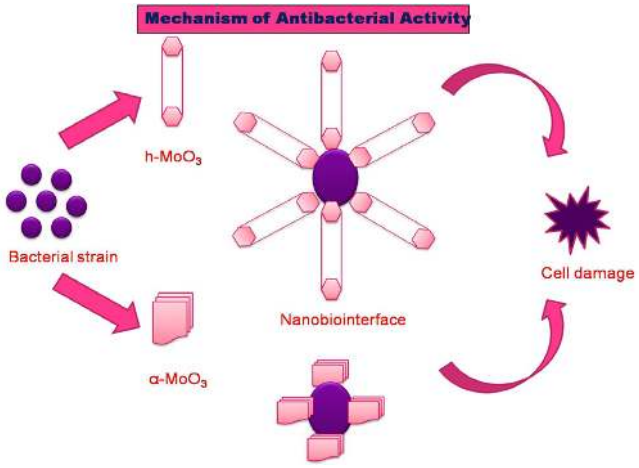

Figure 9: Mechanism of antibacterial activity.

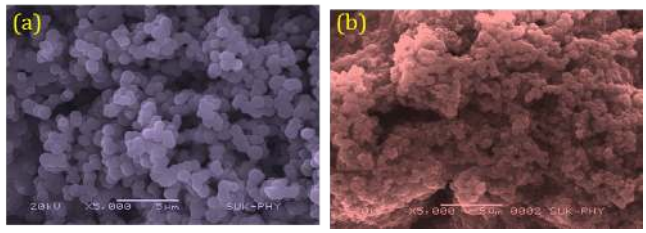

Figure 10: SEM image of *S.aureus* before and after exposure to α-MoO_3.

antibacterial activity of MoO_3 is related to the release of hydroxinium ion according to the following reaction [26].

$$MoO_3 + H_2O \longrightarrow H_2MoO_4$$

$$H_2MoO_4 + 2H_2O \longrightarrow 2H_3O + MoO_4^{2-}$$

Initially the molybdenum trioxide reacts with the water to form molybdic acid. This molybdic acid comes in contact with the water to release the hydroxnium ion. These hydroxinium ions again transformed into the molybdic acid at equilibrium. According to this reaction mechanism MoO_3 should be in contact with water for antibacterial activity (Figure 10).

To further confirm the antimicrobial activity of MoO_3 nanoparticles SEM images were taken to determine the changes in the cell morphology of *S. Aureus*. The Figure 10a shows normal circular shaped cells with intact cell membrane. On the other hand Figure 10b shows the cells are shrunk and deformed after exposure to MoO_3 nanoparticles. This fact indicates the cell damage of bacteria [46,47] thus confirming the antibacterial activity of MoO_3 nanoparticles. All these discussion suggest that studying the direct surface interaction between the metal oxide nanoparticles and bacterial species leading to the cell death. All these aspects are really important for further investigations. The designing of nanomaterials with multiple mechanisms of antibacterial action provides a new paradigm in the fight against resistant bacterial species.

Conclusions

In the proposed research work, we have successfully synthesized hexagonal MoO_3 via chemical bath deposition method. MoO_3

exhibited phase transformation from hexagonal to orthorhombic after annealing. XRD study confirms hexagonal and orthorthombic phase for as synthesized and annealed sample respectively. The as synthesized MoO_3 shows well oriented hexagonal rods assembled together to form sea urchin like architecture. This morphology reveals better intercalation chemistry and anisotropic growth mechanism. After annealing, the one dimensional hexagonal nanorods were transformed into two Dimensional plates like structures. Hence herein, we are reporting one 1D as well as 2D morphology for MoO_3. The XPS analysis of both samples concludes Mo with (+6) oxidation state and oxygen with (-2) oxidation state. HRTEM images confirms highly crystalline nature of sample. Both the phases of MoO_3 exhibit good antibacterial activity against two bacterial species *Streptococcus aureus* and *Bacillus megaterium* whereas α-MoO_3 exhibits good antibacterial activity against gram negative *E. coli*. The phenomenon of nanobiointerface is also important in order to study the antibacterial activity of nanocrystalline MoO_3. Thus antibacterial activity of MoO_3 is an innovative approach for the destruction of micro-organisms in hospitals and public places.

Acknowledgement

One of the authors Ms. Neha Desai is thankful to UGC, New Delhi for providing financial assistance through UGC Major Research Project Ref. No. F 41-301/2012(SR).

This work is also supported by Basic science research programme through the National Science Research Foundation of Korea (NRF) funded by Ministry of education (NRF-2009-0094055).

References

1. Nakata K, Fujishima A (2012) TiO2 Photocatalysis: Design and Applications. J Photochem Photobiol C 13: 169-189.
2. Horiuchi Y, Toyao T, Takeuchi M, Matsuoka M, Anpo M (2013) Recent advances in visible-light-responsive photocatalysts for hydrogen production and solar energy conversion--from semiconducting TiO2 to MOF/PCP photocatalysts. Chem Phys 15: 13243-13253.
3. Luo X, Deng F, Lin L, Luo S, Guo B, et al. (2013) Facile one- step synthesis of inorganic-framework molecularly imprinted TiO2 /WO3 nanocomposite and its molecular recognitive photocatalytic degradation study of target contaminant. Environ Sci Technol 47: 7404-7412.
4. Li Y, Hsu P, Chen S (2012) Multifunctional biosensors at WO3-TiO2 modified Electrode for photoelectrocatalysis of norepinephrine and riboflavin. Sensor Actuat Chem 174: 427-435.
5. Zhang L, Li Y, Zhang Q, Wang H (2013) Hierarchical nanostructures of WO3 nanorods on TiO2 nanofibers and their enhanced visible light photocatalytic activity for degradation of organic pollutants. Cryst Eng Comm 15: 5986-5993.
6. Illyaskutty N, Kohler H, Trautmann T, Schwotzer M, Pillai VP (2013) Enhanced ethanol sensing response from nanostructured MoO_3: ZnO thin films and their mechanism of sensing. J Mater Chem C 1: 3976-3984.
7. Luo W, Fu XK, Ma LH (2007) The research on high quality TiO. MoO_3 doped WO_3 electrochromic film. Chin Chem Lett 18: 883-886.
8. Galatsis K, Li YX, Wlodarski W, Comini E, Sberveglieri G, et. al. (2002) Comparision of single and binary oxide MoO. TiO. WO_3 sol-gel gas sensors. Sensor Actuat B Chem 83: 276-280.
9. Pandeeswari R, Jeyaprakash BG (2014) Nanostructured Î±-MoO3 thin film as a highly selective TMA sensor. Biosens Bioelectron 53: 182-186.
10. Lunk HJ, Hartl H, Hartl MA, Fait MJ, Shenderovich IG, et. al. (2010) "Hexagonal molybdenum trioxide" known for 100 years and still a fount of new discoveries. Inorg Chem 49: 9400-9408.
11. Noerochim L, Wang JZ, Wexler D, Chao Z, Liu HK (2013) Rapid Synthesis of free standing MoO_3/grapheme films by the microwave hydrothermal method as cathode for bendable lithium batteries. J Power Sources 228: 198-205.
12. Chen JS, Cheah YL, Madhavi S, Lou XW (2010) Fast Synthesis of α-MoO3 nanorods with controlled aspect ratios and their enhanced lithium storage capabilities. J Phys Chem C 114: 8675-8678.
13. Huang L, Xu H, Zhang R, Cheng X, Xia J, et. al. (2013) Synthesis, Characteization of g-C_3N_4-MoO_3 photocatalyst with improved photocatalytic activity. Appl Surf Sci 283: 25-32.
14. Yao JN, Yang YA, Loo BH (1998) Enhancement of photochromism and electrochromism in MoO_3/Au and MoO_3/Pt thin films. J Phys Chem B 102: 1856-1860.
15. Di Yao D, Field MR, O'Mullane AP, Kalantar-Zadeh K, Ou JZ (2013) Electrochromic properties of TiO_2 nanotubes coated with electrodeposited MoO3. Nanoscale 5: 10353-10359.
16. Sen UK, Mitra S (2012) Electrochemical activity of α-MoO_3 nanobelts as lithium-ion battery cathode. RSC Adv 2: 11123-11131.
17. Sakaushi K, Thomas J, Kaskel S, Eckert J (2013) Aqueous solution process for the synthesis and assembly of nanostructured one dimensional α-MoO_3 electrode materials. Chem Mater 25: 2557-2563.
18. Fu Q, Chen J, Shi C, Ma D (2013) Room-temperature sol-gel derived molybdenum oxide thin films for efficient and stable solution-processed organic light-emitting diodes. ACS Appl Mater Interfaces 5: 6024-6029.
19. Niederberger M, Krumelch F, Muhr HJ, Muller M, Nesper R (2001) Synthesis and characterization of novel nanoscopic molybdenum oxide fibers. J Mater Chem 11: 1941-1945.
20. Zhang L, Xu Y, Jin D, Xie Y (2010) Well aligned molybdenum oxide nanorods on metal substrate:Solution based synthesis and their electrochemical capacitor application. J Mater Chem 20: 7135-7143.
21. Zhou L, Yang L, Yuan P, Zou J, Wu Y, et al. (2010) α-MoO_3 nanobelts: A high performance cathode material for lithium ion batteries. J Phys Chem C 114: 21868-21872.
22. Liang R, Cao H, Qian D (2011) MoO3 nanowires as electrochemical pseudocapacitor materials. Chem Commun (Camb) 47: 10305-10307.
23. Hajipour MJ, Fromm KM, Ashkarran AA, Aberasturi DJ, Larrmendi IR, et al. (2012) Antibacterial properties of nanoparticles. Trends Biotechnol 30: 499-511.
24. Sonia S, Jayram ND, Suresh Kumar P, Mangalraj D, Ponpandia N et. al. (2014) Effect of NaOH concentration on structural, surface and antibacterial activity of CuO nanorods synthesized by direct sonochemical method. Superlattices and Microstruc 66: 1-9.
25. Vasanthi M, Ravichandran K, Jabena Begum N, Marugnatham G, Snega S, et al. (2013) Influence of Sn doping level on antibacterial activity and certain physical properties of ZnO films deposited using a simplified spray pyrolysis technique. Superlattices and Microstruc 55: 180-190.
26. Zollfrank C, Gutbrod K, Wechsler P, Guggenbichler JP (2012) Antimicrobial activity of transition metal acid MoO(3) prevents microbial growth on material surfaces. Mater Sci Eng C Mater Biol Appl 32: 47-54.
27. Krishnamoorthy K, Veerapandian M, Yun K, Kim SJ (2013) New function of molybdenum trioxide nanoplates: toxicity towards pathogenic bacteria through membrane stress. Colloids Surf B Biointerfaces 112: 521-524.
28. Naganagowda G, Petsom A (2011) Synthesis and antimicrobial activity of oxazolone, Imidazolone and triazine derivatives containing benzothiophene. Bull Korean Chem Soc 32: 3914-3922.
29. Chithambararaj A, Bose AC (2011) Investigation on structural, thermal, optical and sensing properties of meta-stable hexagonal MoO(3) nanocrystals of one dimensional structure. Beilstein J Nanotechnol 2: 585-592.
30. Chithambararaj A, Sanjini NS, ChandraBose A, Velmathi S (2013) Flower like hierarchical h-MoO_3: New findings of efficient visible light driven nanophotocatalyst for methylene blue degradation. Catal Sci Technol 1405-1414.
31. Chithambararaj A, Sanjini NS, Velmathi S, Bose AC (2013) Preparation of h-MoO3 and Î±-MoO_3 nanocrystals: comparative study on photocatalytic degradation of methylene blue under visible light irradiation. Phys Chem Chem Phys 15: 14761-14769.
32. Zheng L, Xu Y, Jin D, Xie Y (2009) Novel metastable hexagonal MoO_3 nanobelts: Synthesis, phtochromic and electrochromic properties. Chem Mater 2: 5681-5690.
33. Wang G, Jiu T , Li P , Li J , Sun C, et al. (2014) In situ growth of columnar MoO_3 buffer layer for organic photovoltaic applications. Org Electron 15: 29-34.
34. Irmawati R, Shafizah M (2009) The production of high purity hexagonal MoO_3

through the acid washing of As-prepared Solids. IJBAS-IJENS 9: 34-36.

35. Wang Y, Zhu Y, Xing Z, Qian Y (2013) Hydrothermal synthesis of a-MoO3 and the influence of later heat treatment on its electrochemicaproperties. Int J Electrochem Sci 8: 9851-9857.

36. Dhage SR, Hassan MS, Bong Yang O (2009) Low temperature fabrication of hexagon shaped h-MoO3 nanorods and its phase transformation. Material Chemistry and Physics 11: 511-514.

37. Sui L, Xu Y, Zhang X, Cheng X, Gao S, et al. (2015) Constructuion of three dimensional flower like α-MoO3 with hierarchical structure for highly sensitive trimethylamine sensor. Sensors and Actuators B Chem 208: 406-414.

38. Yu HL, Li L, Gaoa XM, Zhanga Y, Meng F, et al. (2012) Synthesis and H_2S gas ensing properties of cage like of a-MoO3/ZnO composite. Sensor Actuat B chem 171-172: 679-685.

39. Umbarkar SB, Birdar AV, Mathew SM, Shelke SB, Patil PT, et al. (2006) Vapor phase nitration of benzene using mesoporous MoO3/SiO2 solid acid catalyst. Green Chem 8: 488-493.

40. Deki S, Beleke AB, Kotani Y, Mizuhata M (2009) Liquid phase deposition synthesis of hexagonal molybdenum trioxide thin films, J Solid State Chem 18: 2362-2367.

41. Mao Y, Li W, Sun X, Ma Y, Xia J (2012) Room-temperature ferromagnetism in hierarchically branched MoO_3 nanostructures. Cryst Eng Comm 14: 1419-1424.

42. Alsaifa MYA, Balendhrana S, Fieldb MR, Lathamb K, Wlodarskia W, et al. (2014) Two dimensional α-MoO_3 nanoflakes obtained using solvent-assisted grinding and sonication method: Application for H2 gas sensing Sensor Actuat B chem 192: 196-204.

43. Wang YW, Cao A, Jiang Y, Zhang X, Liu JH (2014) Superior antibacterial activity of zinc oxide/graphene oxide composites originating from high zinc concentration localized around bacteria. ACS Appl Mater Interfaces 6: 2791-2798.

44. Shinde VV, Dalavi DS, Mali SS, Hong CK, Kim JH, et al. (2014) Surfactant free mictrowave assisted synthesis of ZnO microspheres: Study on their antibacterial activity. Appl Surf Sci 307: 495-502.

45. Li H, Cui Q, Feng B, Wang J, Lu X (2013) Antibacterial activity of TiO_2 nanotubes: Influence of crystal phase, morphology and Ag deposition. Appl Surf Sci 284: 179-183.

46. Fan J, Li Y, Nguyen HN, Yao Y, Rodrigues DF (2015) Toxicity of exfoliated-MoS2 and annealedexfoliated-MoS2 towards planktonic cells, biofilms, and mammalian cells in the presence of electron donor. Environ Sci: Nano 2: 370-379.

47. Rajan A, Vilas V, Philip D (2015) Studies on catalytic, antioxidant, antibacterial and anticancer activities ofbiogenic gold nanoparticles. Journal of Molecular Liquids 212: 331-339.